



OPEN

# Multi-resistive Reduced Graphene Oxide Diode with Reversible Surface Electrochemical Reaction induced Carrier Control

SUBJECT AREAS:  
ELECTRONIC PROPERTIES  
AND DEVICES  
ELECTRONIC DEVICES

Received  
19 February 2014

Accepted  
16 June 2014

Published  
10 July 2014

Hyungtak Seo<sup>1,2</sup>, Seungbae Ahn<sup>3</sup>, Jinseo Kim<sup>1,2</sup>, Young-Ahn Lee<sup>1,2</sup>, Koo-Hyun Chung<sup>4</sup> & Ki-Joon Jeon<sup>3</sup>

<sup>1</sup>Department of Energy Systems Research, Ajou University, Suwon 443-739, Republic of Korea, <sup>2</sup>Department of Materials Science and Engineering, Ajou University, Suwon 443-739, Republic of Korea, <sup>3</sup>Department of Environmental Engineering, Inha University, 100 Inha-ro, Nam-gu, Incheon, 402-751, Republic of Korea, <sup>4</sup>School of Mechanical Engineering, University of Ulsan, Ulsan 680-749, Republic of Korea.

Correspondence and requests for materials should be addressed to H.S. (hseo@ajou.ac.kr) or K.-J.J. (kijeon@inha.ac.kr)

The extended application of graphene-based electronic devices requires a bandgap opening in order to realize the targeted device functionality. Since the bandgap tuning of pristine graphene is limited to 360 meV, the chemical modification of graphene is considered essential to achieve a large bandgap opening at the expense of electrical properties degradation. Reduced graphene oxide (RGO) has attracted significant interest for fabricating graphene-based semiconductors since it has several advantages over other forms of chemically modified graphene; such as tunable bandgap opening, decent electrical properties, and easy synthesis. Because of the reduced bonding nature of RGO, the role of metastable oxygen in the RGO matrix is recently highlighted and it may offer emerging ionic devices. In this study, we show that multi-resistivity RGO/n-Si diodes can be obtained by controlling the RGO thickness at a nanometer scale. This is made possible by (1) a metastable lattice-oxygen drift within bulk RGO and (2) electrochemical ambient hydroxyl (OH) formation at the RGO surface. The effect demonstrated in a p-RGO/n-Si heterojunction diode is equivalent to electrochemically driven reversible electronic manipulation and therefore provides an important basis for the application of O bistability in RGO for chemical sensors and electrocatalysis.

Extensive studies have been performed to pursue the application of graphene to electronic devices because of its superior electronic properties. Upon chemical vapor deposition on a metal<sup>1</sup> (e.g., Cu) or epitaxial growth on a SiC substrate<sup>2</sup>, single layer graphene (SLG) shows the highest mobility of any material with a two dimensional (2D) monolayer of sp<sup>2</sup>-bonded carbon atoms. Because of this reason, SLG is physically classified as a zero-bandgap Dirac material<sup>3</sup>. Although the electrical properties of SLG are ideal for electrodes, the utmost interest in graphene is to transform it to a semiconductor for achieving the various functionalities required from electronic device components. A representative example related to this issue is the graphene-channel transistor. In order to meet the modern low-power transistor specifications, the on/off current ratio should be at least  $>10^6$ <sup>3</sup>. However, the best result on graphene transistors revealed a value of  $<10^2$  for the on/off current ratio<sup>4</sup>. This problem with graphene transistors is essentially associated to the lack of a sufficient bandgap for device functionality<sup>5</sup>. There have been various approaches to achieve a bandgap opening in graphene, such as bilayer graphene (A-B stacking)<sup>6</sup>, structural modifications<sup>7</sup>, and chemical functionalization using adsorbed molecules<sup>8,9</sup>. Among these approaches, RGO has been widely researched upon since it is easy to fabricate and offers large bandgaps (e.g.  $\sim 3$  eV)<sup>10,11</sup>. It is obvious that the in-plane electrical conductivity of graphene oxide (GO) is significantly less than that of pristine graphene<sup>12</sup> since O 2p orbitals form sp<sup>3</sup> bonds as a result of the breakup of sp<sup>2</sup> carbon bonds<sup>11</sup>. Nevertheless, RGO with a large bandgap and decent carrier mobility, as compared to GO, has been proven to be suitable as a 2D semiconductor for functional electronic devices such as photoluminescent devices, and highly sensitive optical<sup>12</sup> and chemical sensors<sup>13</sup>. In recent researches on RGO properties, the interaction between graphene and oxygen has attracted significant interest. It has been well established that O-bonded graphene shows p-type electronic characteristics. This was easy to establish since O or water adsorption on the graphene surface from air exposure for several days leads to p-type doping of graphene<sup>14</sup>. More interestingly, this p-type character is easily modified to n-type upon vacuum annealing involving O-related molecule desorption. Y. Sato



*et al.* reported that O adsorption/desorption on a bilayer graphene surface can be controlled by a vertical gate bias in a field effect transistor structure; this observation has been declared as electrically modified charge doping effect<sup>15</sup>. On the basis of these precedent studies, it is clear that the graphene O bond has some degree of bistability, which can be controlled by a relatively low external energy source such as a low electric field and heat. Therefore, the reliable control of graphene O can be a strategy for realizing graphene-based electronic devices. It was recently proved that the use of O bistability in a graphene/Cu junction combined with electric-field-driven out-of-plane O migration provides a resistive switching operation across a nanometer-scale junction<sup>16</sup>. It is thought that O bistability in graphene originates from the unique chemical bonding structure of 2D carbon layers. In-plane electrochemical reduction and oxidation of GO has been demonstrated in a previous study<sup>17</sup>. A great advantage of O bistability control through out-of-plane O migration upon the application of an electric field is that the local change of O in the range of several atomic distances at a very low potential is not a “local chemical change” but equivalent to “global charge doping,” affecting the entire electronic properties of single- or multilayered graphene.

In view of the perspectives of O-bistability in graphene, as claimed in previous reports described above, the present study demonstrates that multiresistivity RGO/n-Si diodes can be obtained by controlling the RGO thickness at the nanometer scale. This is made possible by (1) the electrochemical metastable lattice-O drift within bulk RGO and (2) ambient hydroxyl group (OH) adsorption on the RGO surface. For a typical Schottky-diode structure consisting of p-type RGO/n-Si, a triple bias-dependent modulation of the forward current conductivity is observed. On the basis of electrical analysis under controlled air, vacuum, and nitrogen atmospheric conditions, it is found that the internal lattice-O ion drift and electrochemical OH-group adsorption/desorption in the RGO layer, thin enough for an electrically driven ion drift, act as (1) charge injection barrier and (2) strong p-type doping enhancer, respectively. Therefore, this finding provides an important basis for the application of O bistability toward realizing RGO-based diodes and chemical sensors.

## Results and Discussion

Thickness-controlled RGO films were fabricated on a preheated Si substrate by spin coating. From the height analysis of the step edges of RGO by quantitative atomic force microscope, the resultant RGO film thicknesses were measured to be about 390 and 5.7 nm for the thick and thin films, respectively (Figs. 1a–b). Raman scattering can be employed to directly probe the formation of RGO. Raman G, D, and 2D bands of the thin RGO sample are shown in Fig. 1c. Both the G and 2D modes shift to significantly higher frequency upon oxidation, which is a strong evidence of RGO formation. The in-depth chemical properties of thick and thin RGO and full GO (FGO) were investigated using X-ray photoelectron spectroscopy (XPS). Figure 2a shows C 1s spectra with Gaussian-fitting deconvolution for each sample. In the C 1s XPS spectra, C–C (~284.5 eV), C–O/C = O (~286.8 eV), and C–OOH (~288.7 eV) bonds are resolved by peak deconvolution. The peak assignment was based on a previous analysis of FGO films<sup>18</sup>. Depending on the sample, there are distinctive bonding energy shifts; compared to thick RGO, (1) thin RGO shows a higher bonding energy of the C–C bond, possibly originating from a contribution of partial C–OH bonds, and (2) FGO shows a higher bonding energy of the C–O bond, possibly originating from a contribution of partial C = O bonds with a higher O-coordination of the C species. In order to clarify the trend of bonding states for each sample, the O/C stoichiometric ratio and C 1s bond fractions are plotted in Figs. 2c and 2d, respectively. As expected, the C–O/C = O fraction in FGO is the highest since more O is incorporated. An increase in the O/C stoichiometric ratio from 0.4 in thick RGO to

0.9 in FGO is observed. The C–OOH bond fraction is, however, highest at 18% for thin RGO compared to 5–6% for thick RGO and FGO. Because the same deposition method was applied for thin and thick RGO films, except that the spin coating conditions were varied for thickness control, the higher level of OH incorporation in thin rather than in thick RGO films is believed to originate from different surface conditions. The process conditions for thin RGO provide a more favorable surface to water adsorption and its subsequent dissociation into OH groups bound to C in graphene. In addition, the relative surface portion in the whole film, where water adsorption/dissociation from air or solution occurs, significantly differs between two samples. Typically, the surface oxygen and water adsorption is limited at the top several nm-thick region and this inherently leads to OH/O-rich surface dominant thin RGO layer compared to the thick RGO film where the chemistry of entire film is not highly affected by the surface composition. The degree of water adsorption may also be related to the surface roughness as a key factor to provide the reactive sites (i.e., epoxy group configuration) for O adsorption<sup>11</sup>. Therefore, this proves that the surface of thin RGO is intrinsically or thermodynamically subject to the thermodynamic water dissociation and OH incorporation in RGO. In addition, the important implication of OH-rich RGO is strong p-type electronic conductivity, which affects the RGO diode structures significantly.

The valence band edge XPS spectra (Fig. 1b) indicate that RGO has a significant metallic contribution of an sp<sup>2</sup> C–C bonding configuration, resulting in an overlapping of the Fermi energy level ( $E_F$  level, i.e., 0 eV binding energy) with the valence band onset, while  $E_F$  is ~2 eV above the valence band onset in FGO. This result implies that an incomplete O-coverage of the surface results in partial metallic behavior; this finding is in agreement with an earlier report on the significant bandgap modulation of RGO<sup>19</sup>. GO can be either a p-type or an n-type semiconductor, depending on the environment and the substrate<sup>20</sup>; however, p-type behavior is more common under ambient conditions, suggesting that O<sub>2</sub>/water adsorption plays a role in the p-type character of RGO. The considerably less mobility than pristine graphene as a result of sp<sup>3</sup> C–O bond formation is unavoidable in RGO; nevertheless, this mobility drop can be mitigated by a large bandgap opening.

A log I–V plot for thin and thick RGO/n-Si diodes is shown in Fig. 3a. The diodes show clear rectifying junction characteristics with rectification factors of 64 and 4 for thin and thick RGOs, respectively, at a bias of ±1 V. The inset of Fig. 3a shows the structure of the RGO/n-Si diode used in this study. The Ag electrode offers a good ohmic contact to RGO, which is in contrast to the slightly rectifying junction for FGO (see Supplementary Information, Section 1). Therefore, the rectification occurring at the RGO/n-Si diode is truly related to the interfacial band alignment of the RGO/n-Si junction. Although the forward current in the thick RGO diode seems to exhibit a normal behavior when compared to regular Schottky diodes, the thin RGO diode shows abrupt current saturation at a relatively low voltage of ~1 V. This current saturation is not due to a series resistance between RGO and Ag, which is a common reason for forward current saturation in typical Schottky diodes, since the thick RGO diode with an identical ohmic Ag/RGO contact did not show a similar current saturation. Furthermore, the high bias up to 20 V in thick RGO did not show such an abrupt current saturation at all (see Supplementary Information, Section 2). In order to understand this peculiar phenomenon in the I–V characteristics of the thin RGO diode, an in-depth analysis of charge transport was performed on the basis of the I–V results. Considering the charge transport through an RGO/n-Si junction, tunneling (i.e., direct tunneling, DT, or Fowler-Nordheim, FN) is highly possible for thin RGO/n-Si since the average thickness of RGO is on the order of several nanometers. The tunneling current and applied bias voltage are expressed by the following equations<sup>21</sup>:

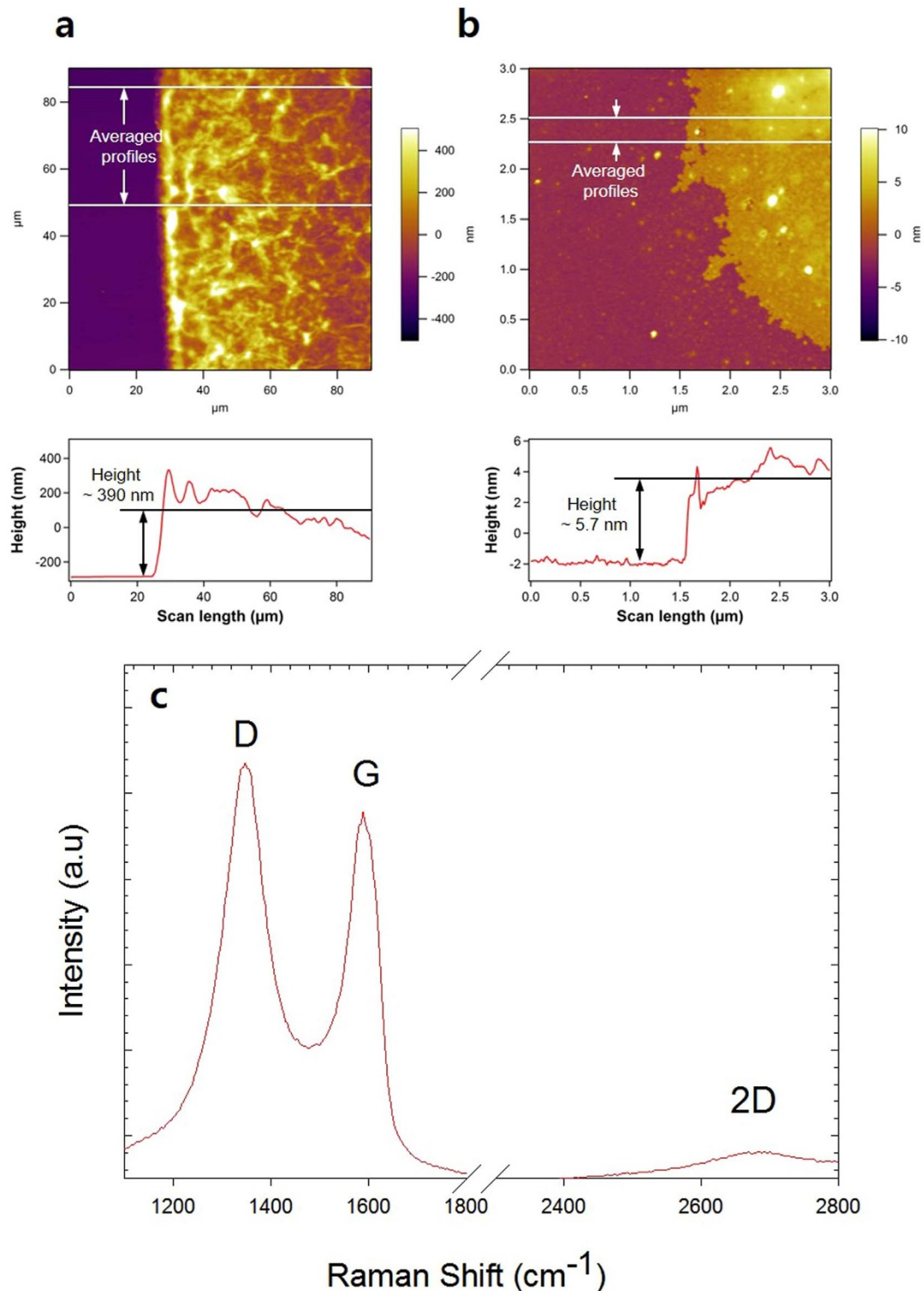


**Figure 1** | AFM images of (a) thick (~390 nm) and (b) thin (~5.7 nm) RGO layers. (c) Raman spectra for a thin RGO layer.

$$I_{OC} \begin{cases} V \exp\left(-\frac{2d\sqrt{2m^*\phi}}{\hbar}\right) & (V < V_{trans}) : \text{Direct tunneling} \\ V^2 \exp\left(-\frac{4d\sqrt{2m^*\phi^3}}{3\hbar v_F}\right) & (V > V_{trans}) : \text{FN tunneling} \end{cases}, \quad (1)$$

where  $m^*$  is the effective mass of an electron,  $\Phi$  is the barrier height,  $d$  is the thickness of RGO,  $e$  is the unit electrical charge, and  $\hbar$  is Planck's constant. Typically, in tunneling current measurements, a

transition from DT to FN tunneling takes place at a transition voltage ( $V_{trans}$ ) defined as  $V_{trans} = \Phi/e$ .  $V_{trans}$  can be found from either a plot of  $\ln(1/V^2)$  versus  $\ln(1/V)$  (i.e., a DT plot) or a plot of  $\ln(1/V^2)$  versus  $(1/V)$  (i.e., FN plot). Figure 3b shows a forward current DT plot for thin and thick RGO/n-Si diodes. For thin RGO/n-Si diodes, an inflection point is observed, where the initial DT current ( $0 < V < 0.4$  V) transforms to an FN current at  $\sim 1$  V. It has been established that in nanoscale junctions using carbon nanotubes<sup>22</sup>,  $\pi$ -conjugated molecules<sup>23</sup>, and Si nanosheets<sup>21</sup>, the charge transport undergoes

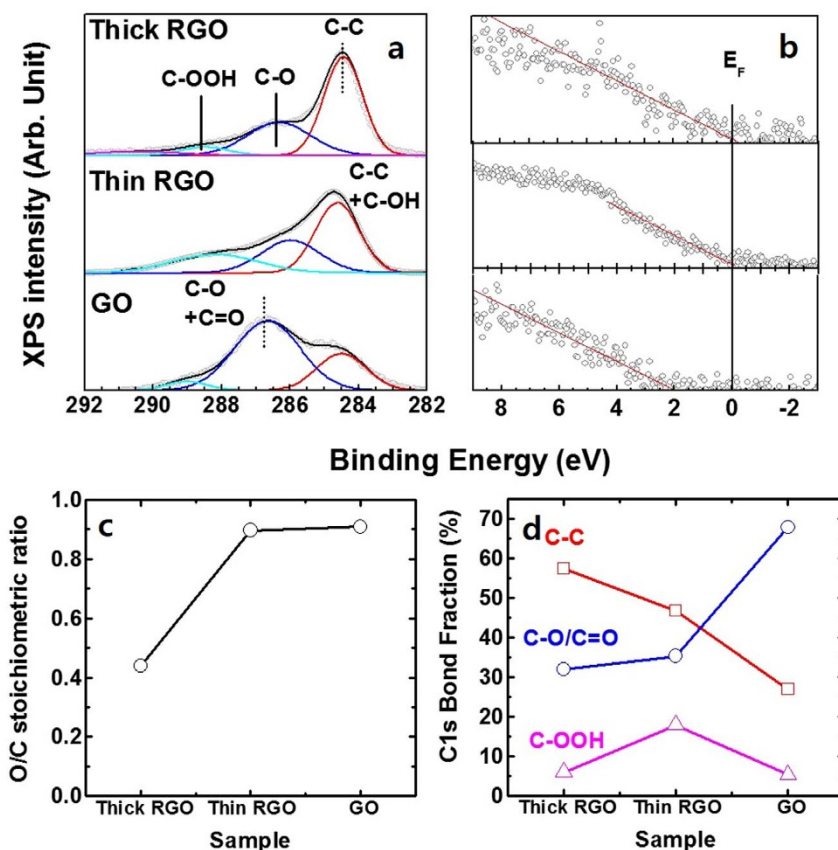


**Figure 2** | XPS spectra for (a) C 1s and (b) VB edge for thick and thin RGO and GO. (c) The O/C stoichiometric ratio and (d) the C 1s bond fraction (C-C, C-O/C=O, and C-OOH) for thick and thin RGO and GO samples.

consecutive transitions from (i) DT to (ii) FN to (iii) final breakdown. This trend is also observed for epitaxial graphene/graphene oxide junctions<sup>20</sup>. The DT plot shown in Fig. 3b follows the same charge transport behavior up to 1 V as reported in other studies; however, above 1 V, abrupt current saturation governed by second DT transport phase (i.e., DT (II)) is induced. Therefore, the thin RGO/n-Si diode has a striking multimode transition in charge transport—DT (I) → FN → DT (II)—disobeying the single charge transport transition (DT → FN) observed in typical nanoscale junction diodes. DT (II) occurs only in a thin RGO diode, implying a relation to the dimensional confinement that results in a dynamic tunneling barrier dependent on an electric field (E field). On the other hand, a thick RGO diode shows a significantly different transport mechanism that is more likely based on Schottky emission (SE) at different slopes at

low and high bias respectively, as shown in the inset of Fig. 3b. The low linear slope of high bias (at  $>2$  V) in SE plot might be due to the partial ohmic resistance. Other tunneling transport mechanisms are excluded for thick RGO because of its thickness of 390 nm. Based on the figure of merit for general tunneling mechanism, under assumption of same effective mass of electrons between two samples, tunneling probability exponentially depends on thickness as expressed by  $\exp(-t_{\text{thick RGO}}/t_{\text{thin RGO}})$  equal to  $\sim 10^{-30}$ . Therefore, no tunneling in thick RGO is readily expected. This is confirmed in the inset of Fig. 3b and its transport mechanism is governed by Schottky emission not by tunneling.

A thin RGO diode shows more interesting changes in the I-V characteristics when a high bias voltage is applied. Figure 4 shows the I-V curve for a thin RGO/n-Si diode for bias voltages up to 10 V

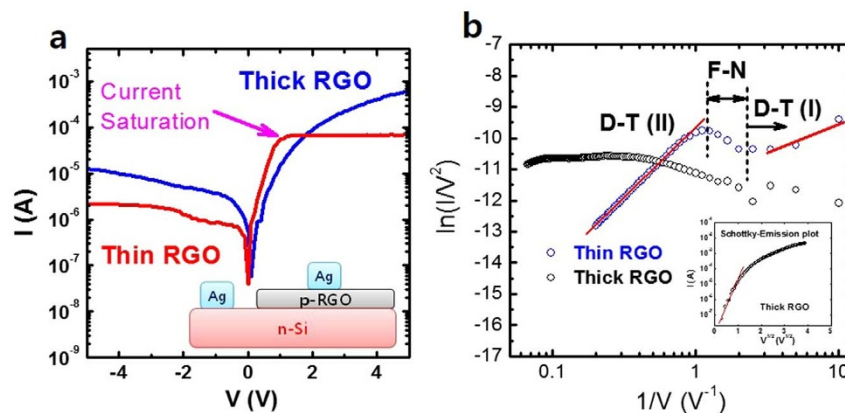


**Figure 3** | (a) A typical I-V curve on the logarithmic current scale and (b) DT plot for thin and thick RGO/p-Si diodes. The inset figures in (a) and (b) are the schematic illustrations of the RGO/n-Si diode structure and a Schottky-emission plot for a thick RGO diode, respectively.



under two different ambient conditions—air and  $N_2$ . Under both ambient conditions, current saturation occurs at  $\sim 1$  V. However, in air, the current rises again from the saturated current level above  $\sim 4$  V. In contrast, no current rise is observed in the  $N_2$  environment. The DT plot indicated that charge transport in the current increase region ( $>4$  V) is most likely due to DT transport. On the basis of the diode dependence on ambient conditions, two crucial conclusions are drawn: (i) the current saturation onset at 1 V is due to intrinsic properties of the diode, regardless of the atmosphere, and (ii) at a high bias voltage, electrically induced reactions between the surface of a thin RGO diode and gas species (only in air) can be considered as a strong modifier of the charge transport. The dependence of the conductivity change in a thin RGO diode on the ambient gas is significant:  $\times 10$  difference in the DT (II) region and  $\times 100$  difference in current rise region ( $>4$  V). In thick RGO diode, same I–V curves were measured both in Air and  $N_2$  ambient without any current saturation as in thin RGO (Data not shown here).

A mechanism for the multimode transition of charge transport in the thin RGO/n-Si diode is proposed, as shown in Fig. 5a. We first consider the possible physical origin of the current saturation onset and the DT (II) region. From Fig. 3b, it is inferred that a bias-induced tunneling barrier is formed at onset voltage and this barrier is distinguished from the tunneling barrier of the DT (I) region. Because this is related to the intrinsic properties of the diode, it is highly possible that negative O ion migration in RGO under an E field forms the new tunneling barrier for the DT (II) region. Recently, S. Kwon *et al.* reported that metastable O ions in ultrathin Cu/single layer graphene junctions (on the scale of several nanometers) can be reversibly drifted by E field control, and also suggested on the basis of density functional calculations that reversible O migration can be accessed via metastable O sites on the graphene surface<sup>16</sup>. Interestingly, the reversible change in resistance due to O ion drift has also been observed at a bias voltage of  $\sim 1$  V<sup>15</sup>, which is equal to the current saturation voltage in this study. Another theoretical study<sup>24</sup> predicted that gate voltage control of O diffusion is possible by the creation of metastable weak bonding from additional electrons supplied by the gate bias, thereby lowering the diffusion barrier energy (0.15 eV) by an order of magnitude from the measured value (1.5 eV) on the graphene surface in thermal equilibrium<sup>25</sup>. Therefore, due to the electrostatic interaction between E-field and O ions in RGO, the positive bias applied to the Au electrode on RGO surface will move negative O ions electrostatically toward the RGO/Ag junction. This is possible because RGO has a significant amount of unsaturated metastable graphene sites available for O ion migration. However, O ions distributed in thick RGO should migrate over a much longer distance by a factor of 68 than that in thin RGO in order to be reversibly localized at either the surface of RGO or RGO/

Si interface. This requires much higher activation energies of O ion migration due to the higher number of collisions and interactions with lattice atoms than those required in thin RGO. Therefore, this limits the effect of O ions for charge transport change or no DT II region occurs in I–V curve of thick RGO diode.

As a result of the O ion drift, an O-rich region is formed at RGO/Ag interfaces, acting as the transient DT (II) barrier formed at a bias of  $>1$  V. This DT (II) barrier formation/disruption occurs reversibly in a way that the backward bias (from high to low voltage) recovers the original I–V curve, as shown in a hysteresis I–V analysis (Supplementary Information, Section 2). As another supporting evidence for O migration under E-field, the thermal dependence of the I–V characteristics was evaluated in order to measure the thermal activation energy of O-diffusion under E-field condition, as shown in Fig. 5b. The substrate temperature is varied from room temperature to  $100^\circ\text{C}$  in vacuum (at 5 mTorr range) in order to minimize any possible surface reactions from ambient air to focus on charge conduction mechanism under E-field driven O diffusion from RGO. In Fig. 4b, the DT (II) region is eliminated as increasing temperature above  $50^\circ\text{C}$ . A continuous current increase is observed without the apparent DT (II) region while the DT (I) region and reverse current are almost identical to those observed at room temperature. Therefore, this behavior serves as evidence that O ions near the surface, which are involved in the transient DT (II) barrier formation at room temperature, are thermally more activated under the high E-field condition. At temperatures higher than  $50^\circ\text{C}$ , thermal activation of O ion diffusion and relevant carrier transport becomes more aggressive to result in the forward/reverse current increase at any voltage, thereby losing the rectifying junction characteristics. On the basis of the analysis of Fig. 5b, the temperature-dependent conductance variation can be thought of as a thermal activation process related to OH and O diffusion and relevant carrier transport in RGO. Furthermore, the thermal conductance response is divided into two regions: (i) O-diffusion in low bias (i.e., DT (I) region) and (ii) O-diffusion in high bias (i.e., DT (II) region). Conductance values at 0.5 V and 2 V were considered according to the Arrhenius law as follows:

$$G \propto \exp\left(-\frac{E_A}{k_B T}\right) \quad (2)$$

where  $G$  is the conductivity,  $E_A$  is the activation energy,  $k_B$  is the Boltzmann constant, and  $T$  is the temperature. In this thermal I–V analysis,  $E_A$  is related to thermally activated O diffusion and relevant carrier transport processes in RGO in the presence of an E field. Figure 5c shows the  $\ln(G)$  versus  $1/k_B T$  Arrhenius plot for the thermal dependence of the I–V curve and yields  $E_A$  values of 0.17 and 0.2 eV for the DT (I) and DT (II) regions, respectively. These activation energy values are comparable to the metastable O diffusion barrier energy (0.15 eV) during electron supply, as predicted by calculations<sup>24</sup>. Although thermal reaction can result in complicated chemical/physical changes at such a Si/RGO nanoscale junction, only loosely bound O and OH in RGO can be thermally activated at the temperature range of  $50$ – $100^\circ\text{C}$  under vacuum since all other bonds such as Si–Si, Si–O, and C–C have high bond strengths. Moreover, upon cooling of the diode measured at the elevated temperature in vacuum, I–V characteristic is clearly recovered to the original RGO property. This indicates that the thermal I–V change is not mainly due to thermal desorption of O from RGO, which is the irreversible chemical change. Indeed, O desorption in RGO has been also reported to occur aggressively at only high temperature  $>100^\circ\text{C}$ <sup>26</sup>. We also should mention that thermal process at  $>100^\circ\text{C}$  has already been gone through for RGO formation so its thermal stability can be assured. Then, the thermal change in I–V feature is mainly related to both (1) O migration in RGO and (2) thermally activated charge transport mechanism. Therefore, the activation energy from temperature-varied I–V curve should be also

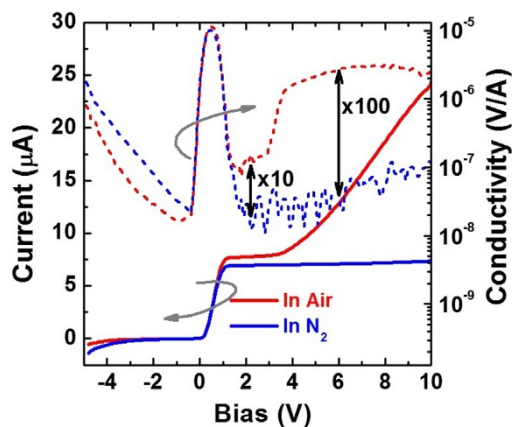


**Figure 4** | Current and conductivity vs. voltage plot for a thin RGO/p-Si diode in air and  $N_2$  atmospheres.

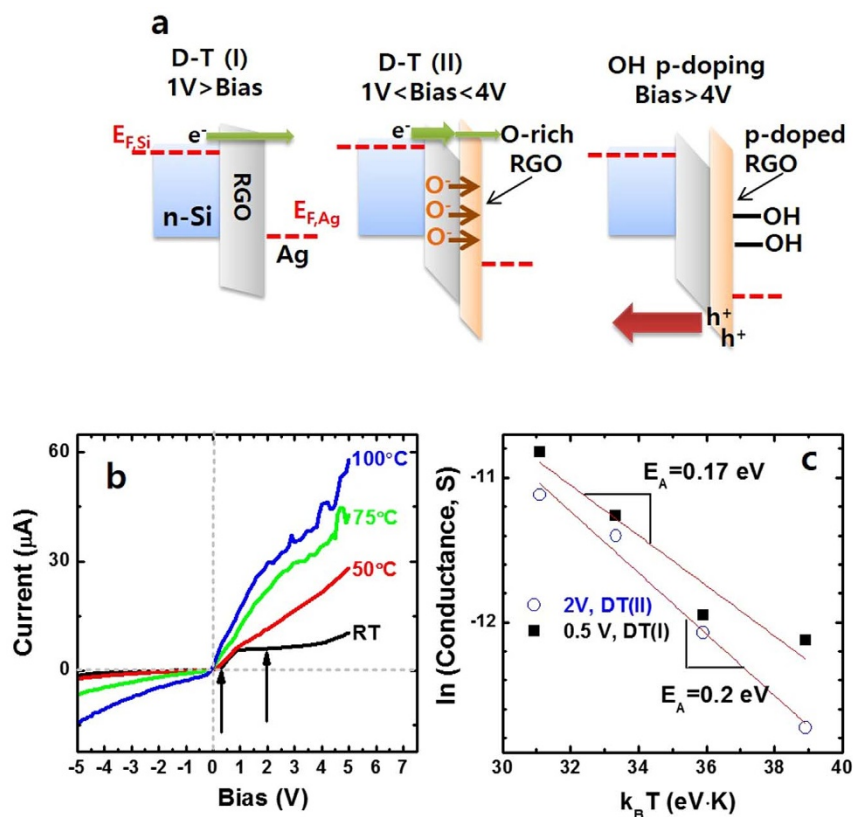


**Figure 5** | (a) Schematic illustration of the charge transport mechanism for each resistivity domain. (b) I–V curve of a RGO/p-Si diode at different temperatures from RT to 100°C and (c)  $\ln(G)$  vs.  $1/k_B T$  Arrhenius plot for bias levels of 0.5 and 2 V.

related to (1) and (2), the major factor of which is not determined clearly at this point. However, O migration under E-field should be mainly or partly involved in the thermal activation process and the activation energy at  $0.17 \sim 0.2$  eV from Fig. 5b is comparable to the reported values of O diffusion barrier on graphene surface under E-field. Therefore, we regard that E-field can lower activation energy greatly in this study. Also, the wiggling I–V trace at the high voltage ( $>2$  V) from  $>75^\circ\text{C}$  indicates a typical transport character of reduced oxides with lots of defect sites (i.e., due to metastable O/OH in RGO). Therefore, it is suggested that Fig. 5b supports that O ion loosely bound C is the main payer for charge transport mechanism in RGO (OH is not a major species due to low bond fraction as shown in Fig. 2d) and it is also controllable by external E-field due to the lowered activation energy extracted from Fig. 5b.

Among possible mechanisms responsible for the second current rise in air following DT (II), RGO surface-gas reactions under an E field or during electron supply are considered the most probable cause. The constituent gas species in air are  $\text{O}_2$ ,  $\text{N}_2$ , and water. A reaction of water and  $\text{N}_2$  is excluded on the basis of the results shown in Fig. 4. A highly possible electrochemical reaction of  $\text{O}_2$  and water at the RGO surface with a high density of electrons under a bias is expressed as follows:



Therefore, as long as this electrochemical reaction proceeds, OH ions can be supplied and adsorbed onto the RGO surface. The p-type electronic doping effect by the hydroxyl group on graphene has been widely studied<sup>26,31</sup>. If OH is chemisorbed on the RGO surface and acts as a p-doping enhancer, it will pull more electrons from carbon atoms, leading to a more positively charged RGO surface. Upon surface OH adsorption, the hole carrier density increases, and concurrently, the current flow by hole injection from RGO to n-Si rapidly increases. If such p-type doping is only limited at surface

or near-surface regions by the OH diffusion length, the hole charge transport can be regarded as charge injection from the OH-rich surface to the RGO bulk until the collection of holes occurs at n-Si. This might lead to complex hole transport at the RGO/p-Si junction, as confirmed by the I–V analysis, revealing no convergence of the current at  $>4$  V to a single charge transport mechanism. Therefore, it is suggested that the controlled multilevel conductivity of RGO is mainly based on a transient electrochemical effect, arising from an E-field-driven lattice O ion drift in bulk RGO and at the RGO/n-Si and RGO/metal interfaces. For electrochemical OH induced p-type doping observed in thin RGO, this requires high flux of electrons with high kinetic energies to ensure over-potential to initiate electrochemical reaction. The number of high energy electrons (i.e., hot electrons) is much higher in thin RGO than in thick RGO due to tunneling process in the short distance less than carrier mean free path but in thick RGO, major portion of electrons is should be thermalized due to electron-lattice scattering (i.e., ion and phonon scattering). This explains why second current rise is not observed in thick RGO even upon applying high voltage up to  $\sim 20$  V. An RGO diode should be stable and reversible for practical applications such as chemical sensors and photodiodes. This aspect was studied on the basis of the hysteresis I–V analysis, showing a current deviation between forward and reverse sweeps only within the DT (II) region (Supplementary Information, Section 3). This is regarded as an indication of the electrochemically modulated current in the voltage region where OH formation/disruption according to Le Chatelier’s principle and bidirectional lattice O ion drift occur in a forward/reverse sweep. Therefore, this is analogous to the statistically distributed O/metal ion drift-controlled resistive change in bistable switching oxides/ionic materials<sup>27</sup>. In repeated hysteresis I–V measurements, biasing at 1 V acts as a “reset” voltage for recovery to an identical current level, regardless of the bias sweep direction., If the high- and low-current level in the DT (II) region becomes larger by some orders of



magnitude by device engineering, the hysteresis behavior provides a potential for use as resistive memory. The peculiar variation of the conductivity in this study is considered to be based on a transient electrochemical effect consisting of (i) an E-field-driven lattice O ion drift and (ii) surface OH p-type doping. It should be noted that a similar mechanism for electrochemical reduction/oxidation of GO was proposed such that each half of the reaction between GO and H<sub>2</sub>O forms H<sup>+</sup> ions at the cathode and OH<sup>-</sup> ions at the anode, respectively<sup>28</sup>. These are very interesting and special properties of the RGO/Si diode geometry under the out-of-plane charge transport mode in nanometer-scale thin RGO and provide an important basis for the application of O bistability. This finding can be potentially utilized for RGO-based ionic devices such as chemical sensors in OH-related chemical environment (e.g., pH sensor) and electrocatalysis.

## Methods

Expanded graphite was prepared via microwave-assisted thermal expansion of highly ordered pyrolytic graphite (SPI-2 grade from SPI). A graphene oxide dispersion was synthesized from the expanded graphite using the modified Hummers method and was reduced by the chemical reduction method. A dispersion of GO-hydrazine was prepared by mixing of as-synthesized GO with hydrazine monohydrate, followed by dilution (150 times) with a mixture of DI water and ethanol and sonication for 1 min. The as-prepared RGO dispersion was spray-coated onto a preheated (240°C) n-type doped and chemically cleaned Si wafer and onto a Si wafer with a thermally grown 300-nm-thick oxide layer (Si/SiO<sub>2</sub> wafer), respectively. The resultant RGO thickness was in the range of ~5 nm for the thin layer and several hundred nanometers for the thick layer, respectively, as measured by step height analysis using atomic force microscopy. Raman spectra were recorded in the backscattering configuration using a micro-Raman spectrometer (Labram, ISA Groupe Horiba), equipped with a He-Ne laser (532 nm, ~0.8 mW at the sample). For diode fabrication, the top Ag (100 nm) electrode on RGO was formed by e-beam evaporation and the rear electrode on the p-Si wafer was produced by applying a Ag paste. The chemical bonds of RGO were analyzed using XPS [ESCA Lab-22201, VG] with an Mg source. The binding energy of each element was calibrated using C-C bonds (284.5 eV) in the C 1 s binding state. The electrical characteristics of a diode and a resistor were measured by a vacuum chamber current-voltage (I-V) probe station connected to a Keithley 4200 semiconductor analyzer. I-V analyses were carried out under diverse atmospheres such as vacuum (10<sup>-3</sup> torr), air, and N<sub>2</sub> in order to investigate electrochemical changes of the RGO surface.

- Bae, S. *et al.* Roll-to-roll production of 30-inch graphene films for transparent electrodes. *Nat Nanotechnol* **5**, 574–578 (2010).
- Geim, A. K. & Novoselov, K. S. The rise of graphene. *Nat Mater* **6**, 183–191 (2007).
- Radisavljevic, B., Radenovic, A., Brivio, J., Giacometti, V. & Kis, A. Single-layer MoS<sub>2</sub> transistors. *Nat Nanotechnol* **6**, 147–150, doi:Doi 10.1038/Nnano.2010.279 (2011).
- Lin, Y. M. *et al.* 100-GHz Transistors from Wafer-Scale Epitaxial Graphene. *Science* **327**, 662–662 (2010).
- Kim, K., Choi, J.-Y., Kim, T., Cho, S.-H. & Chung, H.-J. A role for graphene in silicon-based semiconductor devices. *Nature* **479**, 338–344 (2011).
- Zhang, Y. B. *et al.* Direct observation of a widely tunable bandgap in bilayer graphene. *Nature* **459**, 820–823 (2009).
- Han, M. Y., Ozyilmaz, B., Zhang, Y. B. & Kim, P. Energy band-gap engineering of graphene nanoribbons. *Phys Rev Lett* **98**, doi:Artn 206805 Doi 10.1103/Physrevlett.98.206805 (2007).
- Jeon, K. J. *et al.* Fluorographene: a wide bandgap semiconductor with ultraviolet luminescence. *ACS Nano* **5**, 1042–1046, doi:10.1021/nn1025274 (2011).
- Nair, R. R. *et al.* Fluorographene: A Two-Dimensional Counterpart of Teflon. *Small* **6**, 2877–2884, doi:DOI 10.1002/sml.201001555 (2010).
- Eda, G., Fanchini, G. & Chhowalla, M. Large-area ultrathin films of reduced graphene oxide as a transparent and flexible electronic material. *Nat Nanotechnol* **3**, 270–274, doi:DOI 10.1038/nnano.2008.83 (2008).
- Gomez-Navarro, C. *et al.* Atomic Structure of Reduced Graphene Oxide. *Nano Lett* **10**, 1144–1148, doi:Doi 10.1021/NI9031617 (2010).
- Chang, H. X. *et al.* Thin Film Field-Effect Phototransistors from Bandgap-Tunable, Solution-Processed, Few-Layer Reduced Graphene Oxide Films. *Adv Mater* **22**, 4872–+, doi:DOI 10.1002/adma.201002229 (2010).
- Lu, G. H., Ocola, L. E. & Chen, J. H. Gas detection using low-temperature reduced graphene oxide sheets. *Appl Phys Lett* **94**, doi:Artn 083111 Doi 10.1063/1.3086896 (2009).

- Romero, H. E. *et al.* n-Type Behavior of Graphene Supported on Si/SiO<sub>2</sub> Substrates. *ACS Nano* **2**, 2037–2044, doi:Doi 10.1021/Nn800354m (2008).
- Sato, Y., Takai, K. & Enoki, T. Electrically Controlled Adsorption of Oxygen in Bilayer Graphene Devices. *Nano Lett* **11**, 3468–3475, doi:Doi 10.1021/Nl202002p (2011).
- Kwon, S., Seo, H., Lee, H., Jeon, K. J. & Park, J. Y. Reversible bistability of conductance on graphene/CuOx/Cu nanojunction. *Appl Phys Lett* **100**, doi:Artn 123101 Doi 10.1063/1.3694754 (2012).
- Ekiz, O. Ö., Ürel, M., Güner, H., Mizrak, A. K. & Dána, A. Reversible Electrical Reduction and Oxidation of Graphene Oxide. *ACS Nano* **5**, 2475–2482, doi:10.1021/nn1014215 (2011).
- Yang, D. *et al.* Chemical analysis of graphene oxide films after heat and chemical treatments by X-ray photoelectron and Micro-Raman spectroscopy. *Carbon* **47**, 145–152, doi:DOI 10.1016/j.carbon.2008.09.045 (2009).
- Luo, Z. T., Vora, P. M., Mele, E. J., Johnson, A. T. C. & Kikkawa, J. M. Photoluminescence and band gap modulation in graphene oxide. *Appl Phys Lett* **94**, doi:Artn 111909 Doi 10.1063/1.3098358 (2009).
- Wu, X. S. *et al.* Epitaxial-graphene/graphene-oxide junction: An essential step towards epitaxial graphene electronics. *Phys Rev Lett* **101**, doi:Artn 026801 Doi 10.1103/Physrevlett.101.026801 (2008).
- Ikuno, T. *et al.* Electron transport properties of Si nanosheets: Transition from direct tunneling to Fowler-Nordheim tunneling. *Appl Phys Lett* **99**, doi:Artn 023107 Doi 10.1063/1.3610486 (2011).
- Chiu, P. W. & Roth, S. Transition from direct tunneling to field emission in carbon nanotube intramolecular junctions. *Appl Phys Lett* **92**, doi:Artn 042107 Doi 10.1063/1.2838353 (2008).
- Beebe, J. M., Kim, B., Gadzuk, J. W., Frisbie, C. D. & Kushmerick, J. G. Transition from direct tunneling to field emission in metal-molecule-metal junctions. *Phys Rev Lett* **97**, doi:Artn 026801 Doi 10.1103/Physrevlett.97.026801 (2006).
- Suarez, A. M., Radovic, L. R., Bar-Ziv, E. & Sofo, J. O. Gate-Voltage Control of Oxygen Diffusion on Graphene. *Phys Rev Lett* **106**, doi:Artn 146802 Doi 10.1103/Physrevlett.106.146802 (2011).
- Yang, R. T. & Wong, C. Kinetics and Mechanism of Oxidation of Basal-Plane on Graphite. *J Chem Phys* **75**, 4471–4476 (1981).
- Jung, I., Dikin, D. A., Piner, R. D. & Ruoff, R. S. Tunable Electrical Conductivity of Individual Graphene Oxide Sheets Reduced at “Low” Temperatures. *Nano Lett* **8**, 4283–4287, doi:Doi 10.1021/Nl8019938 (2008).
- Waser, R. & Aono, M. Nanoionics-based resistive switching memories. *Nat Mater* **6**, 833–840 (2007).
- Teoh, H. F., Tao, Y., Tok, E. S., Ho, G. W. & Sow, C. H. Electrical current mediated interconversion between graphene oxide to reduced graphene oxide. *Appl Phys Lett* **98**, 173105–173103 (2011).

## Acknowledgments

This work was supported by Metrology Research Center funded by Korea Research Institute of Standards and Science (KRISS – 2013 – 13011055), and was also supported by the Basic Science Program (NRF-2012R1A1A1005014, NRF-2014R1A1A1006365) through the National Research Foundation (NRF) of funded by MEST, ICT and Future Planning, Republic of Korea, and by the Basic Science Program (NRF-2009-0094046) through NRF funded by the Ministry of Education, Republic of Korea.

## Author contributions

K.J. and H.S. initiated the idea and outlined the experiments. K.J. and S.A. fabricated RGO samples and performed the electrical and Raman analysis. H.S., J.S. and Y.A.L., performed the XPS analysis. K.H.C. carried out the AFM analysis. H.S. and K.J. performed data analysis and wrote the paper.

## Additional information

**Supplementary information** accompanies this paper at <http://www.nature.com/scientificreports>

**Competing financial interests:** The authors declare no competing financial interests.

**How to cite this article:** Seo, H. *et al.* Multi-resistive Reduced Graphene Oxide Diode with Reversible Surface Electrochemical Reaction Induced Carrier Control. *Sci. Rep.* **4**, 5642; DOI:10.1038/srep05642 (2014).



This work is licensed under a Creative Commons Attribution-NonCommercial-NoDerivs 4.0 International License. The images or other third party material in this article are included in the article's Creative Commons license, unless indicated otherwise in the credit line; if the material is not included under the Creative Commons license, users will need to obtain permission from the license holder in order to reproduce the material. To view a copy of this license, visit <http://creativecommons.org/licenses/by-nc-nd/4.0/>